# RIGOROUS PHOTOGRAMMETRIC PROCESSING OF HIGH RESOLUTION SATELLITE IMAGERY

**Dieter FRITSCH, Dirk STALLMANN**
Institute for Photogrammetry (ifp), Stuttgart University, Germany
Geschwister–Scholl–Strasse 24D, D–70174 Stuttgart
Dieter.Fritsch@ifp.uni-stuttgart.de
Dirk.Stallmann@ifp.uni-stuttgart.de

Working Group IV/4

**KEY WORDS:** remote sensing, orientation, calibration, accuracy

## ABSTRACT

This paper deals with investigations on the geometric reconstruction and sensor calibration of satellite–based optical imaging systems using linear arrays in pushbroom mode, like SPOT, IRS–1C and MOMS–2P/PRIRODA. The geometric model of the sensor is based on an extension of a SPOT model developed by V. Kratky. This geometric solution combines the principle of rigorous photogrammetric bundle formulation with additional constraints derived from known relations assuming an elliptic orbit. The attitude parameters are modelled by a simple polynomial model being linear or quadratic. Ephemeris data (orbital position and attitude data) are not necessary but are optional. The parameters of the interior orientation, e.g. focal length and principle point coordinates, are determined by self–calibration. The sensor model can be easily extended to process images from other high resolution imaging systems as they become available. The flexibility and very good accuracy of the solution will be demonstrated with MOMS–2P/PRIRODA imagery, since multiple scenes with overlapping images are available with a relatively high image resolution.

## 1 INTRODUCTION

Past and current optical sensors like SPOT, IRS–1C/1D and MOMS–02 use linear arrays in pushbroom mode. These systems provide panchromatic and multispectral image acquisition with a geometric resolution between 5 and 20m ground sampling distance. Stereographic coverage is provided by along–track (MOMS–02) or across–track (SPOT) image data collection. New and future systems like IKONOS–2 and QuickBird will have improved features, especially an higher geometric resolution, up to 1m in panchromatic and 4m in multispectral mode with a better dynamic radiometric range. In addition high precision orbital position and attitude data will be provided by the on–board Global Positioning System (GPS) receivers, Inertial Measurement Units (IMU) and star trackers. This additional information allows for reducing the number of ground control points. Furthermore, this information enables direct georeferencing of the imagery without geometric reconstruction of the imaging process (photogrammetric triangulation) and ground control. These developments offer new posibilies for the derivation of follow–ups like digital surface/terrain models, orthoimages and classification maps. Nevertheless to provide accurate and reliable products the calibration and verification of the whole sensor system, consisting of the imaging (camera), position and attitude sensors, is necessary. For this tasks we suggest an extended bundle adjustment for reconstruction of the exterior orientation and point determination with self–calibration.

In our work the used geometric model is based on an extension of a SPOT model developed by V. Kratky (Kratky, 1989). This geometric solution combines the principle of rigorous photogrammetric bundle formulation with additional constraints assuming an elliptic orbit. The sensor position is derived from known nominal orbit relations, while the attitude variations are modelled by a simple polynomial model (linear or quadratic). For self–calibration two additional parameters are added: the focal length (camera constant) and the principle point correction. The exterior orientation and the additional parameters of the sensor model are determined in a general formulation of the least–squares adjustment (Gauss–Helmert model). The use of additional information, e.g. from supplemented data files is not mandatory, but if this information is available it can be used to approximate or preset some of the unknown parameters.

The current implementation has two main drawbacks. First, the number of images that can be processed simultanously is restricted to single — resection — or stereo images, multi–image processing (block adjustment) is not feasible. And second, for self–calibration only two additional parameters are available. In the new implementation of the geometric sensor model the method is capable to handle any number of images, using orbital position and/or attitude data as observations in the adjustment and a refined camera model for a improved self–calibration.

## 2   RELATED WORK

Many different geometric models of varying complexity, rigour and accuracy have been developed, for example:

(Okamoto et al., 1998) proposed the affine transformation to overcome problems arising due to the very narrow field of the sensor view. But the change of the imaging geometry requires a conversion from the original perspective imagery into an affine projection. The method was applied to SPOT stereo scenes of level 1 and 2.

(El-Manadili and Novak, 1996) suggested the Direct Linear Transformation (DLT) for the geometric modeling of SPOT imagery. The DLT approach does not require parameters of the interior orientation and ephemeris information. The solution is based only on ground control points. This is advantageous for processing the new high resolution satellite images, especially if their sensor model and ephemeris information will not be made available. (Savopol and Armenakis, 1998) applied the DLT model to IRS–1C images and (Wang, 1999) expand the DLT approach by adding corrrections for self–calibration.

The principle of orientation images was used by (Kornus et al., 1999) for the geometric inflight calibration of MOMS–2P imagery. This method is based on extended collinear equations (Ebner et al., 1992). The exterior orientation parameters are determined in the so called orientation images. Between the orientation images the parameters of an arbitary scan line is interpolated using Lagrangre polynomials. For modelling of the interior orientation for each CCD array five parameters are introduced. All unknown parameters are estimated in a bundle block adjustment using threefold stereo imagery. For the determination of the unknown parameters a large number of tie points is required which are automatical measured.

(Gugan, 1986) suggested an orbital parameter model. The collinear equations are expanded by two orbital parameters to model the satellite movement along the path and the earth's rotation: the linear angular changes with time of the true anomaly and the right ascension of the ascending node. The attitude variations are modelled by drift rates. This model was successfully adopted by (Valadan Zoej and Petrie, 1998) and applied for SPOT level 1A and 1B, MOMS–02 and IRS–1C (Valadan Zoej and Javid Foomani, 1999) imagery.

For the photogrammetric triangulation using MOMS–02 imagery — MOMS–02/D2 (Baltsavias and Stallmann, 1996) and MOMS–2P/PRIRODA (Fritsch et al., 1998) — we made good experiences using the program SPOTCHECK+ [1]. This solution was successfully applied on various sensors, e.g. SPOT (Baltsavias and Stallmann, 1992), Landsat TM5 and JERS–1. The approach is based on a photogrammetric strict sensor model. Only ca. 10 ground control points are needed. Furthermore the sensor model can be easily extended to process images from other high resolution imaging systems as they become available.

## 3   BUNDEL ADJUSTMENT

The image data applied in this work is collected as follows. The satellite is moving along a well defined close–to–circular elliptical orbit. In along–track mode the sensor is always pointing to the centre of the earth. The images are taken with a pushbroom scanner sensor using a constant time interval. The images taken have an cylindrical perspective, usually distorted due to attitude variations. A single image consist of a fixed number of consecutive scan lines. Each line has its own time–dependent position and attitude parameters (exterior orientation). Despite of the dynamic character of the image orientation not all six parameters of the exterior orientation can be reconstructed for each line, but these parameters are highly correlated for neighbouring lines.

The very narrow field of the sensor's view results in nearly parallel imaging rays. This causes in a high correlation between the projection centre coordinates and the sensor view angle. Thus these pairs of unknown parameters cannot be separated in an standard bundle solution. For compensation, additional constraints or the usage of orbital position and attitude information is required.

### 3.1   Coordinate Systems

In order to establish a rigorous connection between the image, orbital and the reference system the following 2–D and 3–D coordinate systems are used in the formulation of the adjustment model (see Figure 1).

**PIX** $(c, r)$— Pixel Coordinates. Using raw digital imagery the image coordinates are given by pixel $c$ (column) and scan line $r$ (row) position. These coordinates are converted into image coordinates $(x, y)$ with the a priori knowledge of the linear array position in the image plane and the pixel size.

---

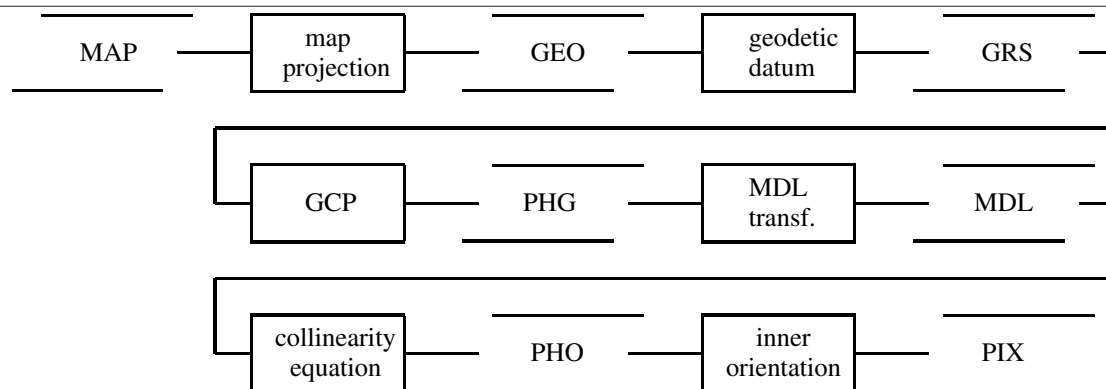[1] In cooperation with the Institute of Geodesy and Photogrammetry, ETH Zurich.

Figure 1: Coordinate transformations.

**MAP** $(E, N, h)$ — Mapping Coordinates. Usually the coordinates of the ground control points are given in 2–D map coordinates $E$ (Easting) and $N$ (Northing) such as Gauss–Krueger or UTM and the orthometric height $H$. Direct and inverse transformations of the map coordinates into ellipsoidal geographic coordinates (geodetic coordinates) with geodetic latitude and longitude are provided by the map projection with the general formulation:

$$E = E(\varphi, \lambda), \quad N = N(\varphi, \lambda) \quad \text{and} \quad \varphi = \varphi(E, N), \quad \lambda = \lambda(E, N).\tag{1}$$

The geodetic coordinates are related to a reference ellipsoid while the orthometric heights are related to a geoid or quasi geoid. If geoidal undulations $N$ are available the orthometric height $H$ can be transfered into the ellipsoidic height $h$ by $h = H + N$.

**GEO** $(\varphi, \lambda, h)$ — Geodetic Coordinates. The geodetic or spatial ellipsoidal coordinates define the point location with respect to a local or global reference ellipsoid. The transformation into cartesian coordinates $X^G$, $Y^G$, $Z^G$ is given by:

$$\begin{pmatrix} X^G \\ Y^G \\ Z^G \end{pmatrix} = \begin{pmatrix} (N + h) \cos\varphi \cos\lambda \\ (N + h) \cos\varphi \sin\lambda \\ [(1 - e^2)N + h] \sin\varphi \end{pmatrix}\tag{2}$$

with

$$N = \frac{a}{\sqrt{1 - e^2 \sin^2\varphi}}.\tag{3}$$

The parameter $N$ is the prime vertical radius of curvature, $e$ is the eccentricity and $a$, $b$ are the semi–major and semi–minor axes of the reference ellipsoid. The inverse transformation can be solved by iterations or in closed form (Vaníček and Krakiwsky, 1986).

**GRS** $(X^{CT}, Y^{CT}, Z^{CT})$ — Geocentric Reference System. The geodetic reference system defines the closest practical approximation of the geocentric natural coordinate system. The origin is located in the mass centre of the earth, with the $Z$–axis going through the Convertional International Origin (CIO), the $XZ$–plane contains the mean meridian of Greenwich and the $Y$–axis going east to complete the right hand system. The geodetic datum defines the position and orientation of the local reference system G in respect to the geodetic reference system CT.

**PHG** $(U, V, W)$ — Photogrammetric Coordinates. The PHG system is a local geocentric coordinate system defined by a fictitous non–existing orbit and the Ground Scene Centre (GSC) with the location $(\varphi_0, \lambda_0, h_0)$. Figure 3 shows the relations between the orbital ellipse and the earth represented by the geodetic reference system GRS. The $U$–axis is normal to the orbital plane, the $W$–axis pointing through the GSC and the $V$–axis completes the right hand system.

**MDL** $(X, Y, Z)$ — Model Coordinates. The MDL system is introduced for computational reasons to achive good numerical stability. MDL coordinates are shifted to coincide with the GSC and scaled to the approximate image size but with the same orientation as the PHG system.

### 3.2 Orbital Geometry

Assume the satellite obeys Kepler's laws and moves along an orbital ellipse (Figure 2). The orbit can be described by the six Keplerian parameters (Slama et al., 1980). These parameters define an ellipse, orient it in relation to the earth and place the satellite on the ellipse at a particular time. The size and shape of the orbital ellipse is defined by the semi–major axis of the ellipse $a$ and the numerical eccentricity $e$. The orientation of the orbital plane against the equator is defined by orbital inclination $i$ and the right ascension of the ascending node . The argument of perigee and the true anomaly or travel angle define the position of the satellite on the ellipse at a particular time $t$.
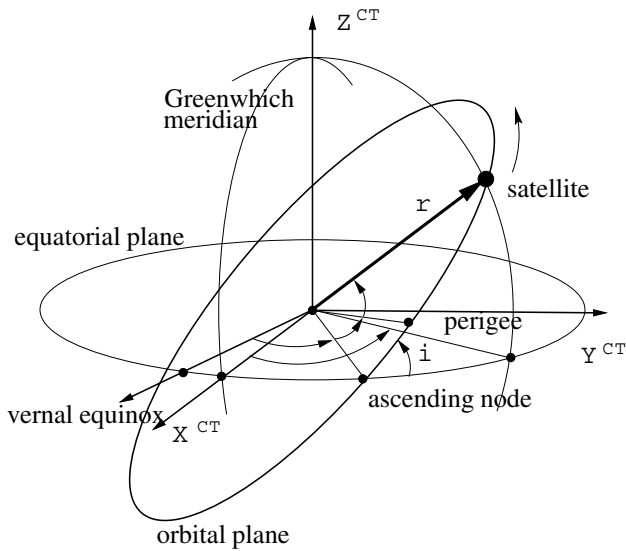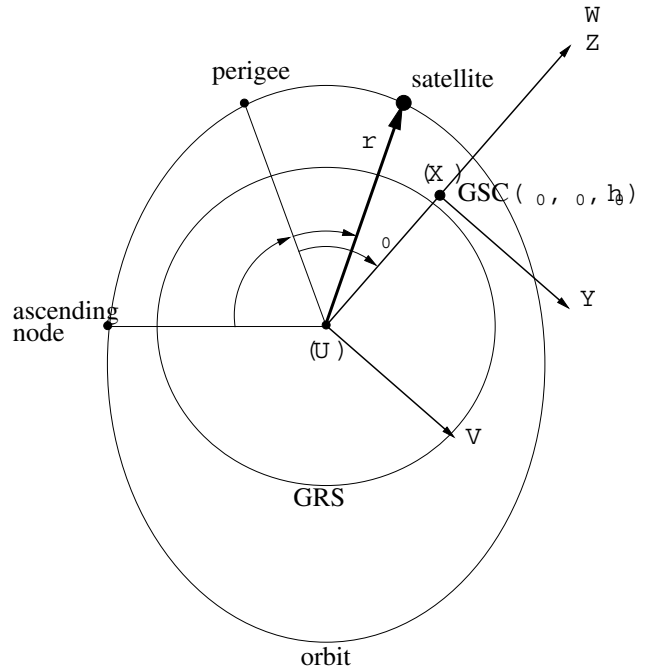
Figure 2: Orbital relations.



Figure 3: Object coordinate systems.

**3.2.1 Satellite Position.** The satellite position is represented by the geocentric vector $r$. In terms of polar coordinates $r$ is defined by the geocentric latitude , the (geographic) longitude and the geocentric radius $r$ as a function of time. Time $t$ is the only independent variable in the orbital relations. Because of the Keplerian character of the satellite motion the travel angle is not direct proportional to the elapsed time. With the knowledge of the mean angular velocity $_m$ the relation between and $t$ is established by the following three equations:

$$\cos E = \frac{e + \cos}{1 + e\cos} \tag{4}$$

$$M = E - e\sin E \tag{5}$$

$$t = M / _m \tag{6}$$

where $E$ is called eccentric anomaly and $M$ mean anomaly. Equation (4) – (6) express the time–to– conversion $= F (t)$. For the opposite task, the –to–time conversion $t = F_t ( )$, the inversion of the Kepler's equation 5 is required. Applying Newton's root–solving method (Slama et al., 1980) to equation 5, $E$ can be computed within a few iterations. Finaly is derived from

$$\cos = \frac{\cos E - e}{1 - e\cos E} . \tag{7}$$

**3.2.2 Earth Rotation Effect.** The combination of satellite travel and earth motion results in a composite motion which causes the satellite ground track on earth. The effect with respect to the travel angle can be expressed by the geocentric latitude and the geographic longitude

$$\sin = \sin( + ) \sin i, \quad \tan _S = \tan( + ) \cos i, \quad = _S + _E . \tag{8}$$

where $\tan _E = _E t$ is the longitude change with the angular velocity of the earth $_E$ . The geographic latitude can be derived from the geocentric latitude by

$$\tan = \frac{a^2}{b^2} \tan . \tag{9}$$

The symbols $a$ and $b$ denote the semi–major and semi–minor axis of the reference ellipsoid.

**3.3 Analytical Formulation**

The total number of unknown parameters is 12 per image. The exterior orientation is modelled by 6 parameters: the reference position $(X_0, Y_0, Z_0)$ and the reference attitude elements $(a, b, )$ both are related to the image centre. Attitude variations are modelled by 6 parameters: the linear $(\dot{a}, \dot{b}, \dot{c})$ and quadratic $(\ddot{a}, \ddot{b}, \ddot{c})$ rates. For self–calibration 2 parameters represent the interior orientation: the change of the principle point $y_p$ and the change of the focal length $f$.

For each ray in a single image we get two collinearity conditions:

$$F_x = \bar{X}z - \bar{Z}x = 0, \quad F_y = \bar{Y}z - \bar{Z}y = 0 \tag{10}$$

where

$(\bar{X}, \bar{Y}, \bar{Z})^T = (X - X_c, Y - Y_c, Z - Z_c)^T$    object coordinates reduced to the projection centre;
$X_c, Y_c, Z_c$                             projection centre coordinates;
$X, Y, Z$                              object coordinates;
$x, y, z$                              "transformed" photo coordinates.

**3.3.1 Exterior Orientation.** The time–dependent perspective centre coordinates are expressed by quadratic polynomials:

$$X_c = X_0 + \dot{X}t + \ddot{X}t^2, \quad Y_c = Y_0 + \dot{Y}t + \ddot{Y}t^2, \quad Z_c = Z_0 + \dot{Z}t + \ddot{Z}t^2 \tag{11}$$

with the reference position $X_0, Y_0, Z_0$ and lineare $\dot{X}, \dot{Y}, \dot{Z}$ respectively quadratic $\ddot{X}, \ddot{Y}, \ddot{Z}$ rates of the sensor position. These rates are computed from rigorous orbital relations.

The "transformed" photo coordinates are defined by an orthogonal transformation of the photo coordinates $(\bar{x}, \bar{y}, \bar{z})$ into a system parallel to the object coordinate system:

$$(x, y, z)^T = T_t T_v (\bar{x}, \bar{y}, \bar{z})^T \tag{12}$$

where the orthogonal transformation consists of a time–dependent rotation matrix of the attitudes $T_t$ and a fixed rotation matrix of the side view angle $T_v$.

The rotation matrix of the attitudes is defined as a function of three off–diagonal matrix elements (Schut, 1958/59)

$$T_t = T (a = a_{12}, b = a_{13}, c = a_{22}) \tag{13}$$

and the three matrix elements are expressed as time–dependent linear or quadratic polynomials:

$$a = a_0 + \dot{a}t + \ddot{a}t^2, \quad b = b_0 + \dot{b}t + \ddot{b}t^2, \quad c = c_0 + \dot{c}t + \ddot{c}t^2 \tag{14}$$

with linear $(\dot{a}, \dot{b}, \dot{c})$ and quadratic $(\ddot{a}, \ddot{b}, \ddot{c})$ rates of the sensor attitudes.

**3.3.2 Inner Orientation.** The concept of inner orientation follows the Manual of Photogrammetry (Slama et al., 1980), by which photo coordinates are defined as follows:

$$\begin{array}{c} \bar{x} \\ \bar{y} \\ \bar{z} \end{array} = \begin{array}{c} x - x_p \\ y - y_p \\ -(f + \Delta f) \end{array} \tag{15}$$

with

$x, y$    image coordinates;
$x_p, y_p$    coordinates of the principle point;
$f, \Delta f$    focal length and change of focal length.

Assuming high accurate calibration of the interior camera orientation, for each pixel the correct image coordinates are available: $c = (x, y)$. For cameras with unknown interior orientation we can simplify $\bar{x} = \bar{x}_0$, futhermore the linear array is assumed to be exactly in the camera center $\bar{x}_0 = 0$.

**3.3.3 Time conversion.** Assuming a known constant scanning rate the time $t$ can be derived directly from the scan fequence $f_s$ by:

$$t = r / f_s \tag{16}$$

where $r$ is the row or line number of the scan line in the strip.

## 3.4 Least–Squares Solution

The mathematical model in equation 10 has the general form $F(L, g) = 0$. In this equation $L$ denotes the observed image coordinates and vector $g$ the unknown parameters (Karara, 1989). Unlike most bundle adjustment programs which are based on the explicit form, i.e. the Gauss–Markov model, the more general Gauss–Helmert model is used here. Since the least–squares solution is applied to a system of non–linear condition equations we have to linearize the contraints using the following linear implicit model:

$$Av + Bg + u = 0, \quad P = Q^{-1} \tag{17}$$

with

$A, B$    design matrices composed of partial derivatives of the collinearity conditions
        with respect to the observations and orientation parameters;
$g$       vector of unknown parameters;
$u$       misclosure vector;
$v$       residuals vector of the observations;
$P$       weight matrix;
$Q$       *a priori* cofactor matrix for the observations.

$F_x$ and $F_y$ is linearized through a Taylor expansion and limited to the first order terms. Splitting matrix $B$, respectively vector $g$ we get:

$$Bg = [B_c \quad B_a \quad tB_a \quad t^2 B_a \quad B_s \quad B_x] [g_c \quad g_a \quad \dot{g}_a \quad \ddot{g}_a \quad g_s \quad g_x]^T. \tag{18}$$

For a single ray we get the following submatrices

$$A = \begin{matrix} Xt_{31} - Zt_{11} & Xt_{32} - Zt_{12} \\ Yt_{31} - Zt_{21} & Yt_{32} - Zt_{22} \end{matrix}, \quad v = \begin{matrix} v_x & v_y \end{matrix}^T \tag{19}$$

$$B_c = \begin{matrix} -z & 0 & x \\ 0 & -z & y \end{matrix}), \quad g_c = \begin{matrix} dX_0 & dY_0 & dZ_0 \end{matrix}^T \tag{20}$$

$$B_a = \begin{matrix} -Zy & -(Xx + Zz) & -Xy \\ Zx & -Yx & -(Yy + Zz) \end{matrix}, \quad g_a = \begin{matrix} da & db & dc \end{matrix}^T \tag{21}$$

$$B_x = \begin{matrix} z & 0 & -x \\ 0 & z & -y \end{matrix}, \quad g_x = \begin{matrix} dX & dY & dZ \end{matrix}^T \tag{22}$$

$$B_s = \begin{matrix} Zt_{13} - Xt_{33} & Xt_{31} - Zt_{11} \\ Zt_{23} - Yt_{33} & Yt_{31} - Zt_{21} \end{matrix}, \quad g_s = \begin{matrix} dx_p & df \end{matrix}^T. \tag{23}$$

The solution is

$$g = -(B^T PB)^{-1} (B^T Pu), \quad P = (AQA^T)^{-1}. \tag{24}$$

Since higher order terms in 17 are neglected, iterations are required to get a better approximation of the solution. After convergence the residuals of the observed image coordinates $v$, the variance factor $\hat{\sigma}_0^2$ and the co–factor matrices $Q_{xx}$, $Q_{vv}$, $Q_{\bar{ll}}$ can be derived during the adjustment.

## 3.5 Orbital Constraints

The narrow field of view effects a weak geometry and introduces high correlations between the unknown parameters, which causes numerical problems, i.e. the adjustment does not converge. To keep the orbital position of the sensor within statistical limits of the expected nominal orbit, three additional constraints derived from known orbital relations and the corresponding weights are used.

   1. The geocentric distance contraint keeps the satellite in orbit:

$$F_r = r^2(X_0, Y_0, Z_0) - r^2(_0) = 0, \quad p. \tag{25}$$

   2. The –offset constraint restrict the movement of the reference position along the orbit:

$$F = (X_0, Y_0, Z_0) - {}_0 = 0, \quad p. \tag{26}$$

3. The  –offset constraint restricts the rotation of the orbital plane:

$$F = (X_0, Y_0, Z_0) - {}_0 = 0, \quad p \quad . \tag{27}$$

The reference values of the nominal orbit $_0$ and $_0$ and the nominal geocentric distance $r^2(_0)$ serves as pseudo–obervations. The geocentric distance $r^2(X_0, Y_0, Z_0)$, the travel angle $(X_0, Y_0, Z_0)$ and the geographic longitude $(X_0, Y_0, Z_0)$ are derived from the unknown reference position.

The constraining functions have the general form $F_c(g, c) = 0$ and contribute to the formation of normal eqations. The linearized form is equivalent to the linear model 17:

$$A_c v_c + B_c g + u_c = 0, \quad P_c = Q_c^{-1} \tag{28}$$

with

| | |
|---|---|
| $A_c, B_c$ | design matrices composed of partial derivatives of collinearity conditions in respect to the pseudo–observations and orientation parameters; |
| $g$ | vector of unknown parameters; |
| $u_c$ | misclosure vector; |
| $v_c$ | residuals vector of the pseudo–observations; |
| $P_c$ | pseudo–weight matrix; |
| $Q_c$ | *a priori* cofactor matrix for the pseudo–observations. |

## 4  TEST DATA

The Modular Optoelectronic Multispectral Stereoscanner MOMS–2P on the Russian space station MIR is a high resolution satellite based imaging system with along–track stereo multispectral imaging capabilities using linear CCDs scanning in pushbroom mode. In 4 different imaging modes various combinations of stereo and multispectral channels can be selected. For stereo evaluations two modes can be used: mode A using two panchromatic fore and aft channels (channel 6 and 7) with 18m and one nadir channel (channel 5) with 6m ground pixel size and mode D using two multispectral nadir looking channels plus two fore and aft channels each with 18m ground pixel size.

Three data takes from three different orbits over Southern Germany were available: T083C, T08C5 and T08FE. The data take T083C was aquired on March 14th 1997 in stereo mode A. Due to strong defocussing of the high resolution sensor channel 5 was not available. T08C5 and T08FE were taken in stereo mode D. The acquisition dates were May 8th 1998 and June 25 1998. The processing level of all three takes are level 1A, i.e. "raw" image data without corrections except for the radiometric improvement. The image quality of all three takes was good (see figure 4). No missing lines exist. The radiometric resoltion was about 7 bits. A strong radiometric preprocessing was not necessary. Only a linear brightness and contrast enhancement was applied.

## 5  PRACTICAL EVALUATION

The Ground Control Points (GCP) were measured in topographic maps of scale 1:25000 and 1:50000 with an accuracy of approx. 5m respectively 10m. The GCPs have been measured monoscopically with an estimated accuracy of 0.5 pixel. The selection of the GCPs were based on their definition (quality) and distribution over the image.

Several versions are calculated using a short (S) orbital segment (scenes 27 and 28), and a long (L) orbital segment (scenes 27 – 30), with a linear (L) or quadratic (Q) attitude model. The results are listed in table 1. 9 respectively 10 and 15 points were used as ground control points. The remaining points are used as check points (CHP) to derive the empirical *accuracy* of the object coordinates ($\mu_X$, $\mu_Y$, $\mu_Z$). Additionally, table 1 shows the standard deviation of unit weight *a posteriori* $\hat{}_0$ and the average *precision* of the object coordinates ($\hat{}_X$, $\hat{}_Y$, $\hat{}_Z$) derived from the inverted normal equations.

Significant differences between the computed versions do not exist. However, as expected, the use of the quadratic attitude model gives slidly better results than the linear model. The average $\hat{}_0$ of 6μm, equivalent to 0.6 pixel (assuming a pixel size of 10μm), confirm the postulated accuracy of the image coordinate measurement of 0.5 pixel. The accuracy derived from check points was 11–14m in planimetry and 13m in height. Compared to accuracies in order of $6 - 7m$ in planimetry and height using MOMS–02/D2 imagery (Baltsavias and Stallmann, 1996) the reached accuracy does not meet our expectations. Moreover, (Kornus et al., 1999) reach accuracies of 8m in planimetry and 10m in height using the same imagery, but with better ground control and an improved sensor model. Also, (Kornus et al., 1999) reports on systematic differences in flight direction which becomes clearly visible in comparison with reference–DTMs.
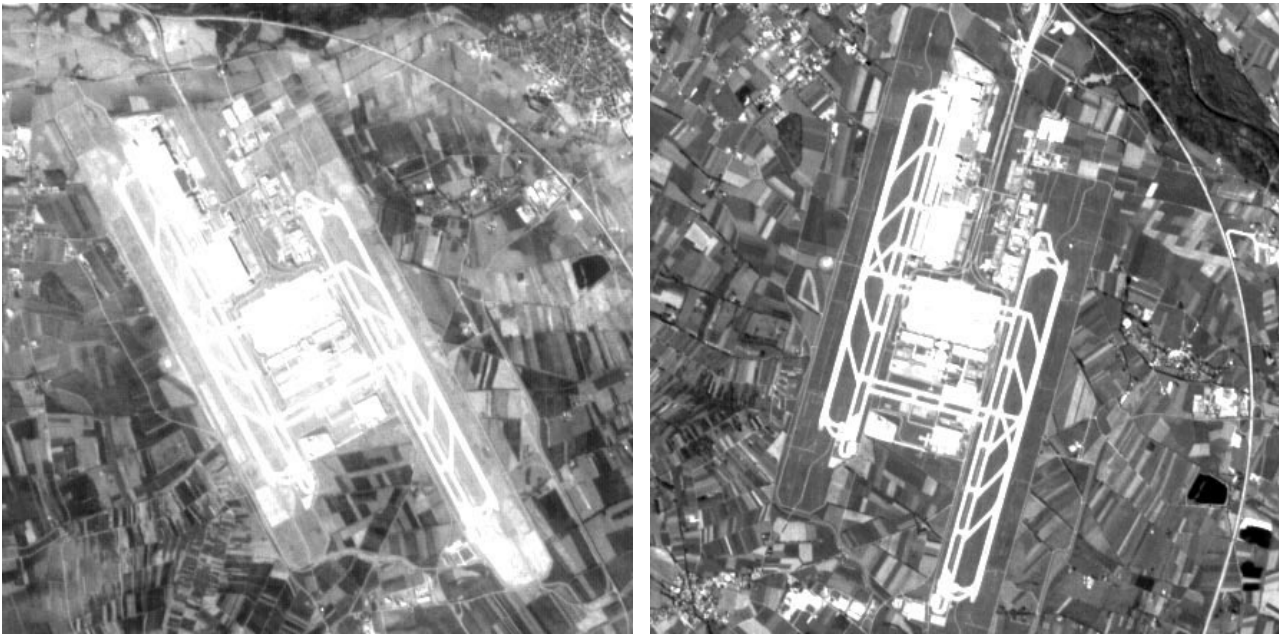
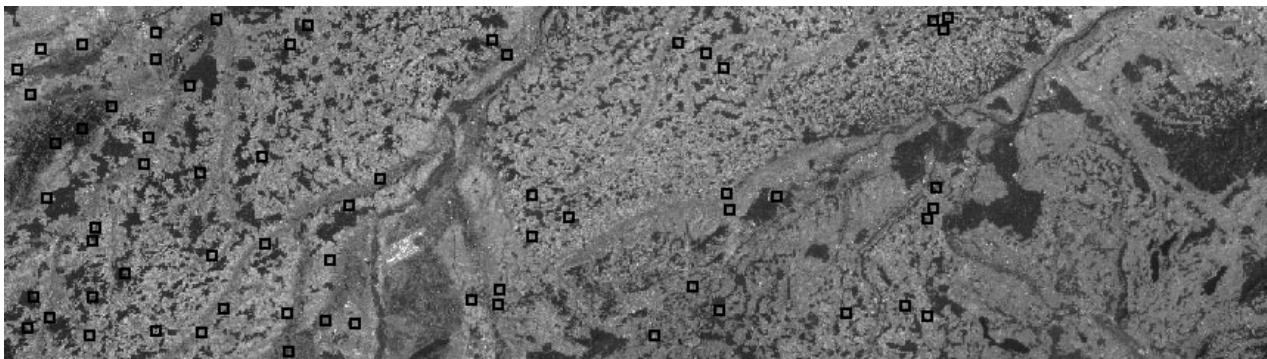Figure 4: Airport Munich in T083C mode A (left) and T08FE mode D (right).



Figure 5: Distribution of the ground control points in data take T083C channel 7.

| Orbit | Model | GCP | CHP | $\hat\sigma_0$ /μm | Precision | | | Accuracy | | |
|---|---|---|---|---|---|---|---|---|---|---|
| | | | | | $\hat\sigma_X$ /m | $\hat\sigma_Y$ /m | $\hat\sigma_Z$ /m | $\mu_X$ /m | $\mu_Y$ /m | $\mu_Z$ /m |
| S | L | 9 | 35 | 6.8 | 10.1 | 7.3 | 8.2 | 14.5 | 12.7 | 12.2 |
| S | Q | 9 | 35 | 6.1 | 7.0 | 5.9 | 6.9 | 11.8 | 13.5 | 13.1 |
| L | L | 10 | 24 | 6.0 | 8.5 | 6.4 | 6.5 | 11.1 | 13.6 | 13.4 |
| L | Q | 10 | 24 | 5.5 | 6.7 | 5.5 | 5.5 | 11.2 | 11.4 | 13.7 |
| L | L | 15 | 20 | 6.0 | 9.1 | 7.5 | 10.1 | 10.4 | 14.1 | 13.0 |
| L | Q | 15 | 20 | 5.7 | 8.8 | 6.0 | 8.8 | 10.1 | 10.5 | 13.8 |

Table 1: Precision and accuracy measures from the bundle adjustment using data take T083C.

## 6   CONCLUSIONS

Using Kratky's simple, fast but strict sensor model an accuracy of 11 – 14m in planimetry and 13m in height can be achived. Only ca. 10 GCPs are required for the orientation of a stereo pair. The reached accuracy of point determination is acceptable for the most applications, e.g.: DTM/DSM generation, ortho image generation, topographic mapping.

Currently none essential modifications in the new implementation of Kratky's sensor model were made. So far, the changes are only related to the coordinate systems, which do not significantly effect the results. Future investigations will make use of an extended self–calibration for the modelling of the interior orientation and the use of more than two images simultaneously.

## REFERENCES

Baltsavias, E. and Stallmann, D., 1992. Metric information extraction from SPOT images and the role of polynomial mapping functions. In: IAPRS, Vol. XXIX, part B4, commission IV, pp. 358–364. ISPRS Congress Washington, D.C.

Baltsavias, E. and Stallmann, D., 1996. Geometric potential of MOMS–02/D2 data for point positioning, DTM and orthoimage generation. In: IAPRS, Vol. XXXI, part B4, commission IV, pp. 110–116. ISPRS Congress Vienna.

Ebner, H., Kornus, W. and Ohlhof, T., 1992. A simulation study on point determination for the MOMS–02/D2 space project using an extended functional model. In: IAPRS, Vol. XXIX, part B4, commission IV, pp. 458–464. ISPRS Congress Washington, D.C.

El-Manadili, Y. and Novak, K., 1996. Precision rectification of SPOT imagery using the direct linear transformation model. Photogrammetric Engineering and Remote Sensing 62(?), pp. 67–72. ISPRS Congress Vienna.

Fritsch, D., Kiefner, M., Stallmann, D. and Hahn, M., 1998. Improvement of the automatic MOMS02–P DTM reconstruction. In: IAPRS, Vol. 32, part 4, pp. 325–330.

Gugan, D., 1986. Practical aspects of topographic mapping from SPOT imagery. The Photogrammetric Record 12(69), pp. 349–355.

Karara, H. (ed.), 1989. Non–topographic Photogrammetry. Second edn, American Society for Photogrammetry and Remote Sensing.

Kornus, W., Lehner, M. and Schroeder, M., 1999. Geometric inflight–calibration by block adjustment using MOMS–2P–imagery of three intersecting stereo-strips. In: Veröffentlichungen des Instituts für Photogrammetrie und Ingenieurvermessungen, Universität Hannover, Nr. 18. Joint Workshop of ISPRS WG I/1, I/3 and IV/4, Sensors and Mapping from Space, Hanover, September 27-30, 1999.

Kratky, V., 1989. Rigorous photogrammetric processing of SPOT images at CCM Canada. ISPRS Journal of Photogrammetry and Remote Sensing 44, pp. 53–71.

Okamoto, A., Fraser, C., Hattori, S., Hasegawa, H. and Ono, T., 1998. An alternative approach to the triangulation of SPOT imagery. In: IAPRS, Vol. 32, part 4, pp. 457–462.

Savopol, F. and Armenakis, C., 1998. Modelling of the IRS–1C satellite pan imagery using the DLT approach. In: IAPRS, Vol. 32, part 4, pp. 511–514.

Schut, G. H., 1958/59. Construction of orthogonal matrices and their application in analytical photogrammetry. Photogrammetria 15(4), pp. 149–162.

Slama, C., Theurer, C. and Henriksen, S. (eds), 1980. Manual of Photogrammetry. Fourth edn, American Society for Photogrammetry and Remote Sensing.

Valadan Zoej, M. and Javid Foomani, M., 1999. Mathematical modelling and geometric accuracy testing of IRS–1C stereo pairs. In: Veröffentlichungen des Instituts für Photogrammetrie und Ingenieurvermessungen, Universität Hannover, Nr. 18. Joint Workshop of ISPRS WG I/1, I/3 and IV/4, Sensors and Mapping from Space, Hanover, September 27-30, 1999.

Valadan Zoej, M. and Petrie, G., 1998. Mathematical modelling and accuracy testing of SPOT level 1B stereopairs. The Photogrammetric Record 16(91), pp. 67–82.

Vaníček, P. and Krakiwsky, E., 1986. Geodesy: The Concepts. Second edn, North–Holland.

Wang, Y., 1999. Automated triangulation of linear scanner imagery. In: Veröffentlichungen des Instituts für Photogrammetrie und Ingenieurvermessungen, Universität Hannover, Nr. 18. Joint Workshop of ISPRS WG I/1, I/3 and IV/4, Sensors and Mapping from Space, Hanover, September 27-30, 1999.